THE ASTRONOMICAL JOURNAL, 122, 2001 NOVEMBER, ASTRO-PH/0108001
Preprint typeset using LaTeX style emulateapj v. 19/02/01

EXPLORATORY CHANDRA OBSERVATIONS OF THE HIGHEST-REDSHIFT QUASARS: X-RAYS FROM THE DAWN OF THE MODERN UNIVERSE

C. VIGNALI,[1] W. N. BRANDT,[1] X. FAN,[2] J. E. GUNN,[3] S. KASPI,[1] D. P. SCHNEIDER,[1] AND MICHAEL A. STRAUSS[3]

Received 2001 June 11; accepted 2001 July 30

ABSTRACT

We report exploratory *Chandra* observations of 14 high-redshift (z=4.06–5.27), optically selected quasars. Ten of these quasars are detected, increasing the number of $z > 4$ X-ray detected quasars by 71%. Our detections include four of the five highest-redshift X-ray detected quasars to date, among them SDSSp J021043.17−001818.4, the highest-redshift ($z = 4.77$) radio-loud quasar detected in the X-ray band. The four undetected objects are the Broad Absorption Line quasars SDSSp J112956.10−014212.4 and SDSSp J160501.21−011220.0, the weak emission-line quasar SDSSp J153259.96−003944.1, and the quasar PSS 1435+3057. A comparison of the quasars' spectral energy distributions (by means of the optical-to-X-ray spectral index, $\alpha_{\rm ox}$) with those of lower-redshift samples indicates that the *Chandra* quasars are X-ray fainter by a factor of ≈ 2. X-ray faintness could be associated with the presence of large amounts of gas in the primeval galaxies harboring these high-redshift quasars, as suggested by recent studies conducted on $z > 4$ quasars in other bands. Using the current *Chandra* data, predictions for the next generation of X-ray observatories, *Constellation-X* and *XEUS*, are also provided.

Subject headings: galaxies: active — galaxies: nuclei — quasars: general — X-rays: galaxies

1. INTRODUCTION

The discovery of quasars at $z > 4$, first accomplished by Warren et al. (1987), has recently been the subject of particular interest because of the first results coming from the Sloan Digital Sky Survey (SDSS; York et al. 2000). In the last few years, the number of known $z > 4.6$ quasars has more than tripled (e.g., Fan et al. 1999a, 2000a; Anderson et al. 2001). About 1000 $z > 4$ SDSS quasars are expected over the next five years, ≈ 100 of which should be at $z > 5$ (Fan 1999; Schneider 1999).

Studies of quasars at the highest redshifts are important for addressing a number of key astrophysical and cosmological issues. High-redshift quasar studies allow investigation of the formation of galaxies and large-scale structures at epochs when the Universe was only 5–10% of its present age (e.g., Efstathiou & Rees 1988; Turner 1991; Small & Blandford 1992; Haehnelt & Rees 1993). From the Eddington limit, luminous quasars are expected to host $\gtrsim 10^{8-9}$ M$_\odot$ black holes. Such objects are probably associated with rare high peaks in the primordial density field, and these peaks should be strongly clustered (e.g., Kaiser 1984). The strong evolution of high-redshift quasars can therefore provide clues about the processes by which the remarkably homogeneous $z \approx 1400$ Universe revealed by the cosmic microwave background is transformed into the inhomogeneous Universe seen today. Furthermore, the emission-line strengths of high-redshift quasars can be used as diagnostics of gas metallicity. If the gas in high-redshift quasars is related to the interstellar material of their young host galaxies, the quasars can be used to constrain the star-formation history and chemical enrichment processes of primordial galactic environments (e.g., Hamann & Ferland 1999; Dietrich & Hamann 2001).

To date, quasars at $z > 4$ have been extensively studied at optical wavelengths (e.g., Schneider, Schmidt, & Gunn 1989, 1991; Kennefick et al. 1995; Kennefick, Djorgovski, & Meylan 1996; Storrie-Lombardi et al. 1996, 2001; Fan et al. 2001), in the radio band (e.g., Schmidt et al. 1995; Hook, McMahon, & Shaver 1999; Stern et al. 2000; Yun et al. 2000) and, to a lesser extent, in the sub-mm and mm range (e.g., McMahon et al. 1994, 1999; Omont et al. 1996a, 2001; Guilloteau et al. 1999; Benford et al. 1999; Carilli et al. 2001). In contrast, our knowledge of the X-ray properties of quasars at $z > 4$ is quite limited. At present, only 14 quasars and one Seyfert galaxy at $z > 4$ have published X-ray detections; three of them are X-ray selected. It has only been possible to obtain X-ray spectra for four $z > 4$ quasars; all four are blazars whose X-ray spectral and variability properties are probably jet-induced (e.g., Moran & Helfand 1997; Yuan et al. 2000; Fabian et al. 2001a,b). The most systematic X-ray study of $z > 4$ quasars has been carried out by Kaspi, Brandt, & Schneider (2000; hereafter KBS) using archival *ROSAT* data. While the most basic X-ray properties of $z > 4$ quasars (e.g., $\alpha_{\rm ox}$, the slope of a nominal power law connecting 2500 Å and 2 keV in the rest frame) appear to be consistent with those of lower-redshift samples, the constraints on their X-ray spectral shapes are still weak.

X-ray studies of the highest-redshift quasars can probe both their central power sources and their environments. Measurement of the intrinsic X-ray continuum's shape, normalization relative to the rest of the spectral energy distribution (SED), and variability can provide information on the inner accretion disk and its corona, and thus ultimately about how the black hole is being fed. There are already some reports that the X-ray continuum shapes of quasars may evolve with redshift at $z \lesssim 2.5$ (e.g., Vignali et al. 1999; Blair et al. 2000); these intriguing results require further study and extension to the highest redshifts. It

[1] Department of Astronomy and Astrophysics, The Pennsylvania State University, 525 Davey Laboratory, University Park, PA 16802 (chris@astro.psu.edu, niel@astro.psu.edu, shai@astro.psu.edu, and dps@astro.psu.edu).

[2] Institute for Advanced Study, Olden Lane, Princeton, NJ 08540-0631 (fan@sns.ias.edu).

[3] Princeton University Observatory, Peyton Hall, Princeton, NJ 08544-1001 (jeg@astro.princeton.edu and strauss@astro.princeton.edu).

TABLE 1
CHANDRA OBSERVATION LOG

Object Name	z	Optical α_{2000}	Optical δ_{2000}	$\Delta_{\rm Opt-X}$ (arcsec)	Obs. Date	Exp. Time (ks)	Ref.
SDSSp J021043.17−001818.4	4.77	02 10 43.2	−00 18 18.4	0.6	2001/01/09	4.95	(1)
SDSSp J021102.72−000910.3	4.90	02 11 02.7	−00 09 10.3	0.3	2001/01/09	4.95	(2)
BRI 0241−0146[a]	4.06	02 44 01.9	−01 34 04.2	0.2	2000/03/11	7.37	(3)
PSS 0248+1802[a]	4.43	02 48 54.3	+18 02 49.2	0.7	1999/12/27	1.73	(4)
BRI 1033−0327[a]	4.51	10 36 23.8	−03 43 19.3	0.9	2000/01/26	3.45	(3)
PSS 1057+4555[a]	4.10	10 57 56.2	+45 55 52.6	0.8	2000/06/14–15	2.81	(5)
SDSSp J112956.10−014212.4	4.85	11 29 56.1	−01 42 12.4	···	2001/03/26	4.88	(6)
SDSSp J120823.82+001027.7	5.27	12 08 23.8	+00 10 27.7	0.6	2001/03/18	4.68	(6)
PC 1247+3406	4.90	12 49 42.2	+33 49 53.9	0.9	2001/03/24	4.68	(7)
PSS 1317+3531[a]	4.36	13 17 43.2	+35 31 32.0	0.3	2000/06/14	3.97	(5)
PSS 1435+3057[a]	4.35	14 35 23.4	+30 57 22.3	···	2000/05/21–22	2.81	(4)
PSS 1443+2724[a]	4.42	14 43 31.2	+27 24 37.0	0.5	2000/06/12	2.17	(4)
SDSSp J153259.96−003944.1	4.62	15 33 00.0	−00 39 44.1	···	2001/03/26–27	5.15	(8–9)
SDSSp J160501.21−011220.0	4.92	16 05 01.2	−01 12 20.0	···	2001/06/24	4.64	(9)

NOTE. — The optical positions of the quasars not found by the SDSS have been taken from the Digital Sky Survey (DSS2).
[a] *Chandra* archival observation.
REFERENCES. — (1) Fan et al. 2001; (2) Fan et al. 1999a; (3) Storrie-Lombardi et al. 1996; (4) Kennefick et al. 1995; (5) Kennefick, Djorgovski, & de Carvalho 1995; (6) Zheng et al. 2000; (7) Schneider, Schmidt, & Gunn 1991; (8) Fan et al. 1999b; (9) Fan et al. 2000a.

is plausible that the X-ray continua of quasars may change at the highest redshifts. If our basic model for quasars is correct, then to be so luminous at such a young age, the highest-redshift quasars may be accreting matter near the Eddington limit where disk instabilities, "trapping-radius" effects, and other energetically important phenomena can arise. Regarding high-redshift quasar environments, there is growing evidence that the fraction of radio-loud quasars (RLQs) characterized by strong absorption in the X-ray band, increases with redshift (e.g., Elvis et al. 1994; Fiore et al. 1998; Reeves & Turner 2000). The absorbing gas is thought to be physically associated with the quasars' environments, perhaps located in the host galaxy or entrained by the radio jets. The situation is far less clear for the radio-quiet quasars (RQQs), which show less of an absorption increase with redshift than do the RLQs (Fiore et al. 1998). However, the constraints on any RQQ absorption-redshift connection are still quite loose and require substantial improvement, especially after the apparent discovery of significant X-ray absorption in some $z \approx 2$ RQQs (Reeves & Turner 2000).

Motivated by these considerations, we have started a project to measure the X-ray properties of the most distant quasars, primarily those found by the SDSS, using the new generation of X-ray observatories. The SDSS multicolor selection method provides a sample of quasars that have been consistently selected in a well-defined manner. The most distant quasar published to date, SDSSp J104433.04–012502.2 at $z = 5.80$ (Fan et al. 2000b), has been successfully detected by *XMM-Newton* (Brandt et al. 2001a; hereafter B01) with a surprisingly low X-ray flux. The main goals of this work are to investigate whether the highest-redshift quasars show different X-ray properties than do local quasars, and to put the results into a comprehensive picture which links these objects to the growth of massive black holes from the first collapsed structures at the end of the cosmic "dark age." The *Chandra X-ray Observatory* is ideal for this program, given its excellent angular resolution coupled with an extremely low background; this combination efficiently allows detection of very faint point sources with relatively low exposure times.

Throughout this paper we adopt an H_0=70 km s^{-1} Mpc^{-1}, q_0=0.5 and Λ=0 cosmology.

2. OBSERVATIONS AND DATA ANALYSIS

2.1. *Chandra observations*

The present sample of high-redshift ($z > 4$), optically selected quasars observed by *Chandra* consists of 14 objects: seven were observed during Cycle 2, while for the remaining seven objects archival data have been analyzed. The observed sample contains many of the $z > 4.8$ quasars known at the time of the *Chandra* Cycle 2 proposal round; the accepted Cycle 2 targets included all but one of the known luminous quasars at $z > 4.8$ without previous or scheduled *XMM-Newton* coverage (as well as one unusual $z = 4.62$ quasar lacking optical emission lines). The sources, along with their redshifts, optical positions, distances between the optical and X-ray positions, observation dates, and dead-time corrected exposure times, are presented in Table 1. In the following text the sources will be referred to through their abbreviated names. The 14 quasars were observed in 13 pointings; SDSS 0210−0018 was serendipitously observed in the field of the quasar SDSS 0211−0009 at an off-axis angle of $\approx 10.3'$.

2.2. *Chandra data analysis*

All of the sources were observed with the *Chandra* Advanced CCD Imaging Spectrometer (ACIS; G. P. Garmire et al., in preparation). ACIS consists of ten CCDs designed for efficient X-ray detection and spectroscopy. Four of the CCDs (ACIS-I; CCDs I0–I3) are arranged in a 2×2 array with each CCD tipped slightly to approximate the curved focal surface of the *Chandra* High Resolution Mirror Assembly (HRMA). The remaining six CCDs (ACIS-S; CCDs S0–S5) are set in a linear array and tipped to approximate the Rowland circle of the objective gratings that can be inserted behind the HRMA. The CCD which lies on-axis in ACIS-S (S3) is orthogonal to the HRMA optical axis. It is a back-illuminated CCD with enhanced sensitivity in the soft X-ray band, and all but one source (the serendipitous one, SDSS 0210−0018, which was detected by the I2 front-illuminated CCD) were observed at its aimpoint. Each CCD subtends an $8.3' \times 8.3'$ square on the sky, and the individual pixels of the CCDs subtend $\approx 0.5'' \times 0.5''$ on the sky. The on-axis image quality of the telescope is FWHM $\approx 0.5''$;

TABLE 2
X-RAY COUNTS IN FOUR ENERGY BANDS

	X-ray Counts			
Object	[0.3–0.5 keV]	[0.5–2 keV]	[2–8 keV]	[0.5–8 keV]
SDSS 0210−0018	< 3.0	$28.0^{+7.0}_{-5.5}$	$7.6^{+4.5}_{-3.0}$	$35.8^{+7.8}_{-6.5}$
SDSS 0211−0009	< 3.0	$5.0^{+3.4}_{-2.2}$	< 3.0	$5.0^{+3.4}_{-2.2}$
BRI 0241−0146	< 6.4	$9.0^{+4.1}_{-2.9}$	< 7.9	$11.9^{+4.6}_{-3.4}$
PSS 0248+1802	$4.0^{+3.2}_{-1.9}$	$9.0^{+4.1}_{-2.9}$	$6.0^{+3.6}_{-2.4}$	$15.0^{+5.0}_{-3.8}$
BRI 1033−0327	$5.0^{+3.4}_{-2.2}$	$8.0^{+4.0}_{-2.8}$	< 6.4	$9.9^{+4.3}_{-3.1}$
PSS 1057+4555	$6.0^{+3.6}_{-2.4}$	$21.0^{+5.7}_{-4.5}$	$6.0^{+3.6}_{-2.4}$	$26.9^{+6.3}_{-5.2}$
SDSS 1129−0142	< 3.0	< 3.0	< 3.0	< 3.0
SDSS 1208+0010	< 3.0	< 4.8	< 4.8	$2.0^{+2.6}_{-1.3}$
PC 1247+3406	< 4.8	$14.0^{+4.8}_{-3.7}$	$3.0^{+2.9}_{-1.6}$	$18.0^{+5.3}_{-4.2}$
PSS 1317+3531	< 4.8	$3.0^{+2.9}_{-1.6}$	< 3.0	$3.9^{+3.1}_{-1.9}$
PSS 1435+3057	< 3.0	< 3.0	< 3.0	< 3.0
PSS 1443+2724	< 3.0	$7.0^{+3.8}_{-3.6}$	< 7.9	$10.0^{+4.3}_{-3.1}$
SDSS 1532−0039	< 3.0	< 3.0	< 6.4	< 6.4
SDSS 1605−0112	< 3.0	< 3.0	< 3.0	< 3.0

NOTE. — Errors on the X-ray counts were computed according to Gehrels (1986). The upper limits are at the 95% confidence level and were computed according to Kraft et al. (1991).

this quantity increases to $\approx 1.0''$ (critical sampling on the detector) at an off-axis angle of $\approx 2'$. Faint and very faint modes were used for the event telemetry format for our observations and the archival observations, respectively; *ASCA* grade 0, 2, 3, 4 and 6 events were used in the analysis. Charge transfer inefficiency (CTI) problems do not significantly affect the present data since all but one of the quasars were observed with the back-illuminated CCD S3. For the quasar SDSS 0210−0018, detected by the I2 front-illuminated CCD, the CTI was mitigated using the latest version of the corrector of Townsley et al. (2000).

As a safety check, we have searched for background flares occurring during the observations. These features are due to "space weather" (primarily soft electrons interacting with the CCDs). The background level is constant to within 10–15% in all the observations. The photon arrival times of all of the sources were also inspected to be certain that they were not produced or affected by "cosmic ray afterglows" (*Chandra* X-ray Center 2000, private communication); note that cosmic ray afterglows are not typically seen on CCD S3. We are confident that the source parameters derived from the analysis described below are unaffected by transient spurious phenomena.

Source detection was carried out with WAVDETECT (Dobrzycki et al. 1999; Freeman et al. 2002). For each image, we calculated wavelet transforms (using a Mexican hat kernel) with wavelet scale sizes of 1, 1.4, 2, 2.8, 4, 5.7, 8, 11.3 and 16 pixels. Those peaks whose probability of being false were less than the threshold of 10^{-6} were declared real; detections were typically achieved for the smaller wavelet scales of 1.4 pixels or less as expected for these distant sources. Source searching was performed in four different energy ranges: the ultrasoft band (0.3–0.5 keV), the soft band (0.5–2 keV), the hard band (2–8 keV) and the full band (0.5–8 keV); these correspond to the $\approx$ 1.7–2.8, 2.8–11, 11–45 and 2.8–45 keV rest-frame bands (at the average redshift of $z \approx 4.6$ for the present sample). Nine of the 14 quasars are detected, and the WAVDETECT photometry results are shown in Table 2. We have cross checked these results with manual aperture photometry; we found good agreement between the two techniques. Five sources went undetected even after increasing the false-positive threshold to 10^{-4}: SDSS 1129−0142, SDSS 1208+0010, PSS 1435+3057, SDSS 1532−0039, and SDSS 1605−0112. The SDSS 1208+0010 ($z = 5.27$) full-band image shows two X-ray photons within $0.8''$ of the optical position of the source. To investigate whether this source can be considered detected, we extracted a 400×400 pixel^2 region centered on the optical position of the quasar (we excluded the immediate vicinity of the quasar itself). This region was covered with 10000 circles of $1''$ radius whose centers were randomly chosen.[4] The counts obtained in each circle were averaged, obtaining 0.0211 counts circle^{-1}. This value was subsequently checked by manually computing the value of the background around the quasar in the same extraction region, finding a very similar value (0.0226 counts circle^{-1}). The Poisson probability of obtaining two counts or more when 0.0211 counts are expected is $\approx 2.2 \times 10^{-4}$.

Recently, using extensive Monte-Carlo simulations on the *Chandra* observation of the Hubble Deep Field North, Brandt et al. (2001b) found that the distribution function of background counts is almost Poisson. We have verified the validity of the Poisson approximation for the SDSS 1208+0010 field using the results of the 10000-circle analysis above. We obtained two counts or more in only two cases. Therefore, the derived probability of obtaining two counts or more is $\approx 2 \times 10^{-4}$, which is similar to the value reported above. In the following, SDSS 1208+0010 will be considered detected by *Chandra* (at about the 3.9σ confidence level for a one-tailed Gaussian distribution).

The situation is more uncertain for SDSS 1532−0039 ($z = 4.62$), an interesting object which shows no emission lines

[4] The on-orbit 80% encircled broad-band energy (EE) radius for on-axis sources is $0.685''$ (see Fig. 6.3 of the *Chandra* Proposers' Observatory Guide). This value has been summed in quadrature with the average positional errors of our clearly detected sources, i.e., the mean difference between the optical and X-ray positions ($\sim 0.6''$). The derived radius is $0.9''$, which we have approximated to $1''$ in order to be reasonably conservative in the EE and positional error estimation. The PSF is quite stable in the sampled region due to its proximity to the optical axis, and the vignetting is negligible.

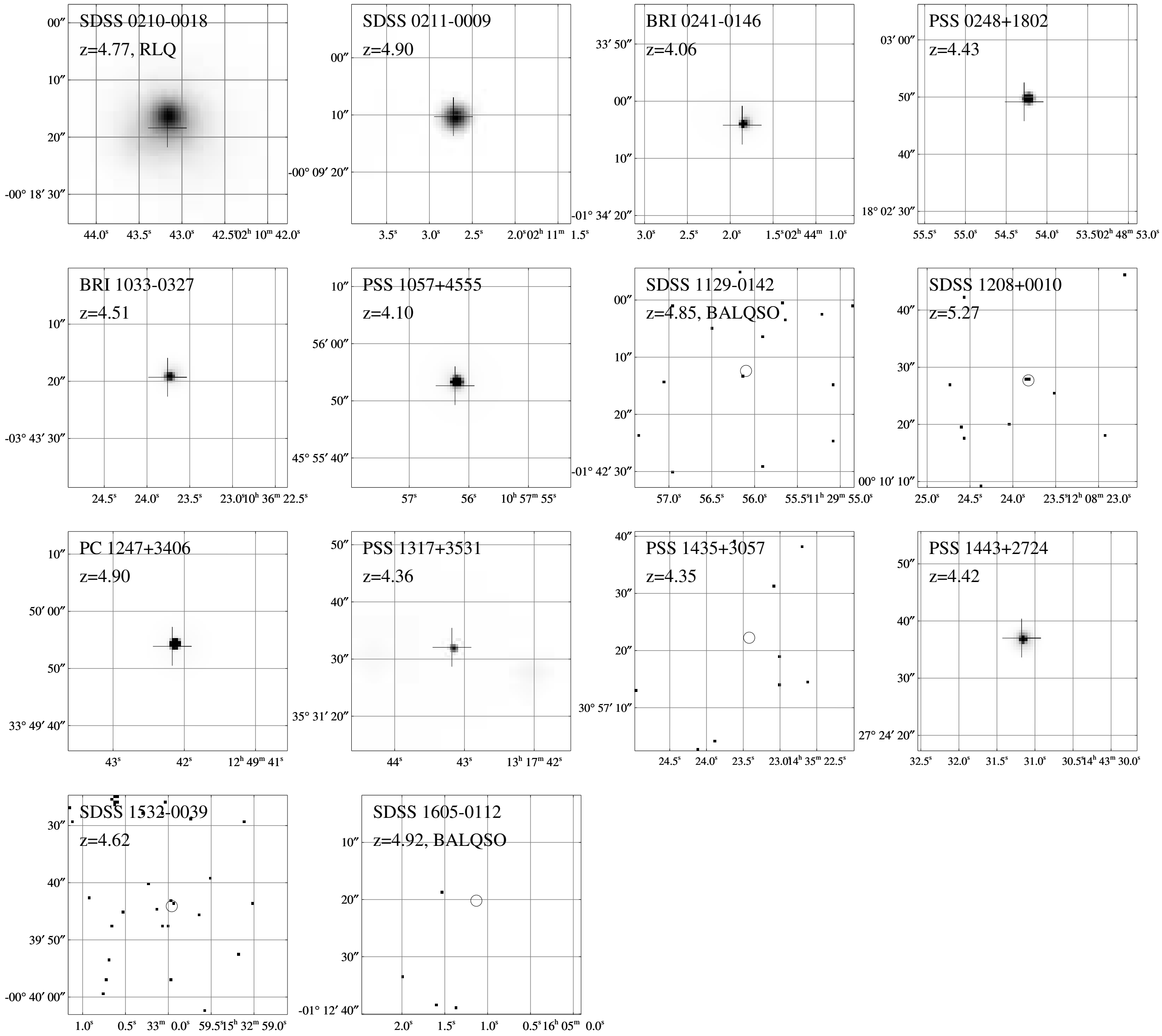

FIG. 1.— *Chandra* full-band images of the 14 high-redshift quasars. In each panel, the horizontal axis shows the Right Ascension, and the vertical axis shows the Declination (both in J2000 coordinates). Each box is $40'' \times 40''$. For the nine sources with the best statistics, a 2σ level of smoothing has been applied; for the other five no smoothing has been done. The optical position is indicated either by a cross or by a circle of $1''$ radius. For SDSS 0210−0018 there is a difference between the source peak and the X-ray centroid of the detection. This is probably due to the large off-axis angle ($\sim 10.'3$) at which the source has been detected.

in its optical spectrum (Fan et al. 1999b, 2000a). WAVDETECT also reports no detection even though aperture photometry reveals two photons within $1.3''$ of the optical position. The local background in this observation is higher than that for the SDSS 1208+0010 observation. By repeating the same procedure applied to the SDSS 1208+0010 field with an extraction circle of radius $1.3''$, the average number of counts in each extraction circle is 0.0757, and the derived Poisson probability of obtaining two or more counts when 0.0757 are expected is $\approx 2.7 \times 10^{-3}$. The Monte-Carlo simulation is in agreement with this value ($\approx 3.2 \times 10^{-3}$).

It is worth noting that for SDSS 1208+0010 and SDSS 1532−0039 the two photons located near the optical position have not been obtained from a blind search across the entire field-of-view, but rather with "a priori" knowledge of the location of the sources. In the following only SDSS 1208+0010 will be treated as having been detected, due to its order-of-magnitude higher statistical significance.

Three other sources have not been detected: the BALQSOs SDSS 1129−0142 ($z = 4.85$) and SDSS 1605−0112 ($z = 4.92$), and the quasar PSS 1435+3057 ($z = 4.35$). Only one photon is present within $1.3''$ of the optical position of SDSS 1129−0142, while no photons were detected for PSS 1435+3057 and SDSS 1605−0112 within $2''$.

Chandra images from 0.5 to 8 keV of the quasars in the sample are shown in Fig. 1. The adaptive smoothing method of Ebeling, White, & Rangarajan (2001) has been applied to the nine images of the sources with clear detections (using a 2σ level of smoothing). For the other five quasars, the raw *Chan-*

dra images are shown. The optical position is indicated either by a cross or by a circle (for the faintest or undetected sources).

To verify that source confusion problems are unlikely, we have computed the number of spurious associations expected at the conservative 0.5–2 keV flux limit of 10^{-15} erg cm^{-2} s^{-1} assuming the integral source counts of Hasinger et al. (1998) and adopting an X-ray error circle radius of $1''$ (see Table 1). We expect $\approx 2.4 \times 10^{-3}$ spurious associations summed over all of the 10 *Chandra* detections.

For the four sources with the most detected counts, SDSS 0210−0018, PSS 0248+1802, PSS 1057+4555 and PC 1247+3406, we computed a band ratio (BR), defined as the ratio between the 2–8 keV and 0.5–2 keV counts. We calculated errors at the $\approx 1\sigma$ level for this quantity following the "numerical method" described in § 1.7.3 of Lyons (1991); this avoids the failure of the standard approximate variance formula when the number of counts is small (see § 2.4.5 of Eadie et al. 1971). For SDSS 0210−0018, PSS 1057+4555 and PC 1247+3406 we found BR=$0.27^{+0.15}_{-0.11}$, $0.29^{+0.19}_{-0.13}$ and $0.21^{+0.21}_{-0.05}$, respectively, which are consistent with unabsorbed $\Gamma \approx 2$ power-law spectra. A flatter $\Gamma \approx 1.5$ power-law slope, as is seen in many RLQs (e.g., Cappi et al. 1997), cannot be ruled out for SDSS 0210−0018 given the statistical uncertainties on the source counts reported in Table 2.

PSS 0248+1802, in contrast, is characterized by a larger band ratio (BR=$0.67^{+0.51}_{-0.34}$). This value corresponds to a power law with $\Gamma \approx 1.2$. If a canonical $\Gamma = 2$ is assumed, an intrinsic H I column density larger than 5×10^{23} cm^{-2} is derived. Given this possible absorption, the prominent soft ($E \lesssim 3$ keV in the rest frame) X-ray emission of PSS 0248+1802 appears surprising, unless a more complex model is adopted. For example, a partial covering model could provide a more reasonable parameterization of its X-ray counts; in this model a fraction of the nuclear radiation is able to escape unabsorbed. Although this model is clearly only a tentative and rough description of the PSS 0248+1802 X-ray spectrum, it is interesting to note that indications of complex X-ray absorbers have recently been obtained for several BALQSOs observed by *Chandra* (Gallagher et al. 2001a) and for the BALQSO SDSS 1044−0125 detected by *XMM-Newton* (B01; Mathur 2001). However, inspection of the optical spectrum (Fig. 3 in Kennefick et al. 1995) shows no evidence for UV BALs in PSS 0248+1802.

We have not carried out a stacking analysis of the *Chandra* RQQs; due to the small number of quasars thus far available, this analysis would be strongly biased toward the three RQQs (PSS 0248+1802, PSS 1057+4555 and PC 1247+3406) with the most detected counts.

2.3. *Simultaneous I-band photometry and spectroscopy*

Given that quasars frequently vary, sometimes spectacularly, in both the optical and X-ray bands, one must always be concerned about the reliability of the frequently employed optical-to-X-ray flux ratio whenever the observations in the two bands of a given quasar are not simultaneous. It is firmly established that there is an anticorrelation between variability and luminosity in the optical band (e.g., Cid Fernandes, Aretxaga, & Terlevich 1996 and references therein). In a recent study Kaspi (2001) shows that high-redshift, high-luminosity quasars ($2 < z < 3.4$) have longer optical variability time scales than low-redshift, low-luminosity quasars ($z < 0.4$), and their variations over ~ 1.5 years (in the rest frame) amount to $\sim 10\%$. For the objects in this study, the observed-frame time between the optical and the *Chandra* observations is about three years; we are helped by the fact that translating this observed temporal difference to the rest frame of the object reduces the delay by a factor of ≈ 5.6, so the typical time elapsed in the rest frame is several months.

Although this is not a large time delay, we have been able to reduce the uncertainty in the optical luminosity at the time of the *Chandra* observations by obtaining *I*-band images and short-exposure, low-resolution spectra within at most two weeks (a few days in the rest frame) for six of the seven quasars observed during Cycle 2. It has been possible to acquire timely optical data on these faint objects by utilizing the queue-scheduled nature of the Hobby-Eberly Telescope (HET; Ramsey et al. 1998).

The data were taken with the HET's Marcario Low Resolution Spectrograph (LRS; Hill et al. 1998a,b; Cobos Duenas et al. 1998). When we were notified that a *Chandra* observation of one of our quasars was to occur in the near future, we activated the object in the HET queue. At the next opportunity (seeing under $3''$, reasonably clear but not necessarily photometric) a short (1–2 minute) *I* image of the quasar field was taken, followed by an ≈ 15 minute spectrum of the quasar.

The image covered a field $\approx 4'$ on a side, and using the published finding charts of the fields it was possible to obtain an approximate photometric calibration using stellar objects in the field. Although it is difficult to give precise estimates given the difference between the LRS and SDSS bandpasses, it is clear that none of the six quasars changed significantly (by $\gtrsim 30\%$) in brightness from their published values, and the spectra also show no significant changes from those published.

3. RESULTS

In Table 3 the X-ray, optical and radio properties of the $z > 4$ quasars observed by *Chandra* are presented. A description is as follows.

Column (1). — The abbreviated name of the source.

Column (2). — The Galactic column density from Dickey & Lockman (1990) in units of 10^{20} cm^{-2}.

Column (3). — The monochromatic rest-frame $AB_{1450(1+z)}$ magnitude (with estimated errors of the order of 0.1 mag).

Columns (4) and (5). — The 2500 Å rest-frame flux density and luminosity. These were computed from the $AB_{1450(1+z)}$ magnitude assuming an optical power-law slope with α=−0.79 ($S_\nu \propto \nu^\alpha$). This α value represents the estimate of the average spectral power-law slope in the rest-frame UV for quasars at $z \approx 4$ obtained by Fan et al. (2001), taking into account the selection completeness of their multicolor sample. Its corresponding 1σ dispersion is 0.34. These values compare to α=−0.91 with dispersion 0.26 from Schneider et al. (1991) and α=−0.93 with dispersion 0.31 from Schneider et al. (2001). These measurements are all significantly steeper than the canonical α=−0.5 median (−0.6 mean) value found by Richstone & Schmidt (1980). Since the majority of their quasars have redshifts below 2, their measurements tend to be made at rest wavelengths considerably longer than those in the region where Fan et al. (2001) and Schneider et al. (2001) determined the continuum properties. Recently, Vanden Berk et al. (2001) derived a composite quasar spectrum from ≈ 2000 SDSS quasars. Their best-fit spectral slope in the range $\approx$ 1300–5000 Å (rest frame) is −0.44 (with an uncertainty of ≈ 0.1 mainly due to the spectrophotometric calibration of the spectra). The steeper indices

TABLE 3

PROPERTIES OF $z > 4$ QUASARS OBSERVED BY *CHANDRA*

Object (1)	$N_{\rm H}$[a] (2)	$AB_{1450(1+z)}$ (3)	f_{2500}[b] (4)	$\log(\nu L_\nu)_{2500}$ (5)	M_B (6)	Count rate[c] (7)	$f_{\rm x}$[d] (8)	$f_{\rm 2keV}$[e] (9)	$\log(\nu L_\nu)_{\rm 2keV}$ (10)	$\alpha_{\rm ox}$[f] (11)	R (12)
SDSS 0210−0018	2.66	19.3	1.06	46.3	−26.8	5.65	$28.1^{+8.1}_{-6.0}$	24.2	45.3	-1.40 ± 0.07	86.1–101.5[g]
SDSS 0211−0009	2.60	20.0	0.56	46.1	−26.2	1.01	$3.1^{+2.2}_{-1.4}$	2.71	44.4	$-1.66^{+0.11}_{-0.12}$	0.6[h]
BRI 0241−0146	3.52	18.4	2.44	46.6	−27.5	1.22	$3.8^{+1.9}_{-1.2}$	2.89	44.3	$-1.89^{+0.09}_{-0.08}$	<1.6[i]
PSS 0248+1802	9.18	18.1	3.21	46.8	−27.9	5.20	$19.6^{+9.0}_{-6.3}$	15.9	45.1	$-1.65^{+0.09}_{-0.08}$	3.0[i]
BRI 1033−0327	4.79	18.8	1.69	46.5	−27.2	2.32	$7.6^{+3.9}_{-2.7}$	6.25	44.7	-1.70 ± 0.09	<0.9[j]
PSS 1057+4555	1.11	17.6	5.09	46.9	−28.3	7.48	$21.6^{+6.5}_{-4.9}$	16.5	45.0	-1.72 ± 0.07	2.5
SDSS 1129−0142	3.60	19.2	1.17	46.4	−26.9	<0.61	<1.6	<1.44	<44.1	<−1.88	<3.3
SDSS 1208+0010	2.00	20.5	0.35	45.9	−25.8	0.43	$1.1^{+1.5}_{-0.7}$[k]	1.02	44.0	$-1.74^{+0.16}_{-0.18}$	<13.1
PC 1247+3406	1.30	19.2	1.17	46.4	−26.9	2.99	$8.7^{+3.2}_{-2.4}$	7.66	44.8	-1.61 ± 0.08	<3.4
PSS 1317+3531	0.99	18.9	1.54	46.4	−27.1	0.76	$2.2^{+2.2}_{-1.2}$	1.74	44.1	$-1.90^{+0.13}_{-0.14}$	<2.1[i]
PSS 1435+3057	1.16	19.1	1.28	46.4	−26.9	<1.07	<2.7	<2.12	<44.2	<−1.83	<2.1[i]
PSS 1443+2724	2.12	19.0	1.40	46.4	−27.0	3.22	$9.7^{+5.5}_{-5.1}$	7.81	44.8	$-1.63^{+0.10}_{-0.14}$	<2.1[i]
SDSS 1532−0039	4.60	19.4	0.97	46.3	−26.7	<1.24	<3.4	<2.86	<44.4	<−1.74	<0.6[h]
SDSS 1605−0112	9.07	19.4	0.97	46.3	−26.8	<0.65	<2.0	<1.77	<44.2	<−1.82	<4.5

[a]From Dickey & Lockman (1990) in units of 10^{20} cm^{-2} .

[b]At rest-frame 2500 Å in units of 10^{-27} erg cm^{-2} s^{-1} Hz^{-1}.

[c]Observed count rate computed in the soft band, in units of 10^{-3} counts s^{-1}.

[d]Galactic absorption-corrected flux in the observed 0.5–2 keV band in units of 10^{-15} erg cm^{-2} s^{-1}.

[e]Rest-frame 2 keV flux density in units of 10^{-32} erg cm^{-2} s^{-1} Hz^{-1}.

[f]Errors have been computed following the "numerical method" described in § 1.7.3 of Lyons (1991); both the statistical uncertainties on the X-ray count rates and the effects of the observed ranges of the X-ray and optical continuum shapes have been taken into account.

[g]FIRST and NVSS report two different values for the flux density: 9.75 ± 0.14 and 11.5 ± 1.0 mJy, respectively.

[h]1.4 GHz flux density from Carilli et al. (2001).

[i]5 GHz flux density from Stern et al. (2000).

[j]1.4 GHz flux density from Yun et al. (2000).

[k]This flux has been computed from the full-band counts and then rescaled to the 0.5–2 keV band.

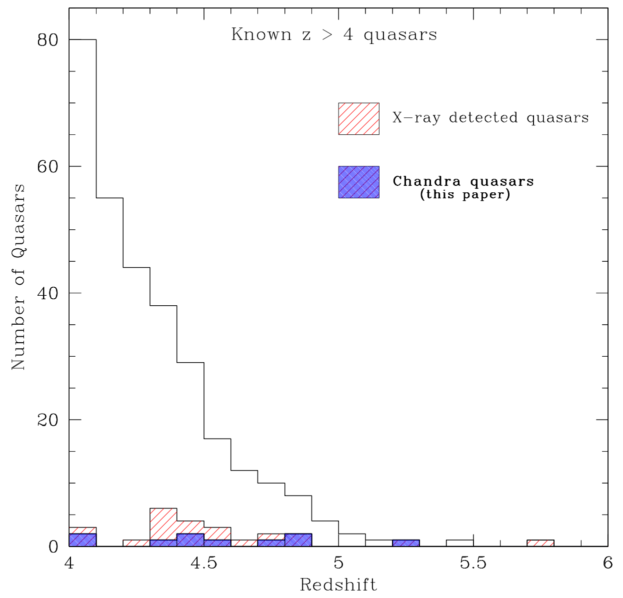

FIG. 2.— Redshift distribution of all known $z > 4$ quasars. The shaded regions indicate the quasars detected in the X-ray band, with particular emphasis on the $z > 4$ *Chandra* detections.

obtained by Fan et al. (2001) and Schneider et al. (2001) may be due to the restricted wavelength range typically used in fitting the continua, as suggested by Schneider et al. (2001), and not to a change in the underlying spectral index at high redshift. We note that changing the optical continuum shape by ≈ 0.3–0.4 has only a weak effect on α_{ox} (see § 4.2).

Column (6). — The absolute B magnitude calculated adopting $\alpha = -0.79$. Given the uncertainty in the continuum shapes of $z \approx 4$ quasars between the rest-frame UV and optical bands (discussed above), a change from $\alpha = -0.79$ to $\alpha = -0.5$ induces an increase of $\approx 40\%$ in the inferred blue luminosity.

Columns (7) and (8). — The observed count rate and the absorption-corrected 0.5–2 keV (observed-frame) flux. The 0.5–2 keV flux was computed using the source counts in the same band and the *Chandra* X-ray Center Portable, Interactive, Multi-Mission Simulator (PIMMS) software (AO3 Version) for a power-law slope of $\Gamma = 2$ ($\Gamma = -\alpha + 1$; $N(E) \propto E^{-\Gamma}$, where $N(E)$ is the number of photons). Samples of nearby RQQs are well fitted in the X-ray band by power-law continua with $\Gamma = 1.7$–2.3 (e.g., George et al. 2000; Mineo et al. 2000; Reeves & Turner 2000). Changing the X-ray spectral slope in the range $\Gamma = 1.7$–2.3 provides only a few percent change in the measured X-ray flux. As a further test, the 0.5–2 keV flux was also computed by converting the full-band counts in the same manner described above. The results are consistent with those tabulated in Table 3 to within 20%. Because SDSS 0210−0018 was detected at a large off-axis angle, its count rate was corrected for vignetting. For the four undetected sources, X-ray upper limits (at the 95% confidence level) were computed following Kraft, Burrows, & Nousek (1991).

Columns (9) and (10). — The rest-frame 2 keV flux density and luminosity. These were computed assuming the same power-law slope as in the count-rate-to-flux conversion.

Column (11). — The optical-to-X-ray power-law slope, α_{ox}, defined as

$$\alpha_{ox} = \frac{\log[(f_\nu(2\,\mathrm{keV})/f_\nu(2500\,\text{Å})]}{\log[\nu(2\,\mathrm{keV})/\nu(2500\,\text{Å})]} \tag{1}$$

where f_ν is the flux density at a given wavelength or energy.

Column (12). — The radio-loudness parameter, defined as $R = f_{5\ \mathrm{GHz}}/f_{4400\ \text{Å}}$ (rest frame). The 5 GHz flux density was computed, unless otherwise stated (see the notes at the bottom of the table), from the NVSS (Condon et al. 1998) or the FIRST (Becker, White, & Helfand 1995) 1.4 GHz flux density assuming a radio power-law slope of $\alpha = -0.8$. The upper limits reported in the table are at the 3σ level. Strong radio-loud objects are usually characterized by $R > 100$, whereas radio-quiet ones have $R < 10$ (e.g., Kellermann et al. 1989). In this regard, the R parameter for SDSS 0210−0018 ($R \approx 86$–102) places it among the RLQ population. It represents the highest-redshift RLQ detected in the X-ray band. The previous highest-redshift X-ray detected RLQ was GB 1428+4217 at $z = 4.72$ (Fabian et al. 1997). Note that the R parameter of SDSS 0210−0018 is much smaller than those of the four $z > 4$ blazars mentioned in § 1; therefore, the fact that SDSS 0210−0018 has a significantly lower X-ray flux than these four blazars is not surprising.

4. DISCUSSION

The capabilities of *Chandra* for efficiently studying the high-redshift X-ray Universe are apparent from Fig. 1. With an average exposure time of ≈ 4.2 ks, 10 out of 14 objects have been detected in the ≈ 3–45 keV rest-frame band, thereby increasing the number of $z > 4$ X-ray detected quasars by 71% (see Fig. 2).[5] Four of the five highest-redshift X-ray detections are presented here. Figure 3 shows that our *Chandra* targets are uniformly distributed in $AB_{1450(1+z)}$ magnitude throughout the high-redshift quasar population. In the following, the X-ray and optical properties of the *Chandra* objects will be compared with those of other high-redshift quasars, primarily the KBS sample (§ 4.1). In § 4.2 the SEDs of the *Chandra* quasars are discussed and compared with samples of optically selected RQQs in order to investigate any possible dependence of quasars' SEDs on redshift or optical luminosity. A discussion of the four quasars which were not detected by *Chandra* is provided in § 4.3.

4.1. *X-ray flux comparisons with other high-redshift quasars*

Figure 4 plots the unabsorbed 0.5–2 keV observed-frame flux versus $AB_{1450(1+z)}$ magnitude for the objects in our *Chandra* sample as well as for objects from the KBS *ROSAT* study and other recent investigations. Because this figure is constructed from *directly observed* physical quantities, it is robust (we present a complementary discussion based on α_{ox}, a parameter somewhat less directly tied to observation, in the next section). KBS only reported 0.1–2 keV fluxes for their quasars (to obtain the highest possible signal-to-noise ratio); to obtain 0.5–2 keV fluxes for these objects we have re-analyzed the archival *ROSAT* data with the MIDAS/EXSAS package (Zimmermann et al. 1998) so that the 0.5–2 keV fluxes could be determined directly from the counts in the exact same band.[6] This was important to obtain the most reliable 0.5–2 keV fluxes possible; converting the KBS 0.1–2 keV fluxes to 0.5–2 keV fluxes assuming a spectral shape is subject to errors in the assumed spectral shape, errors in the Galactic absorption correction, and

[5] The full list of known $z > 4$ quasars is available at http://www.astro.caltech.edu/∼george/z4.qsos.

[6] We have also recalculated the 0.1–2 keV fluxes and obtained good agreement with KBS.

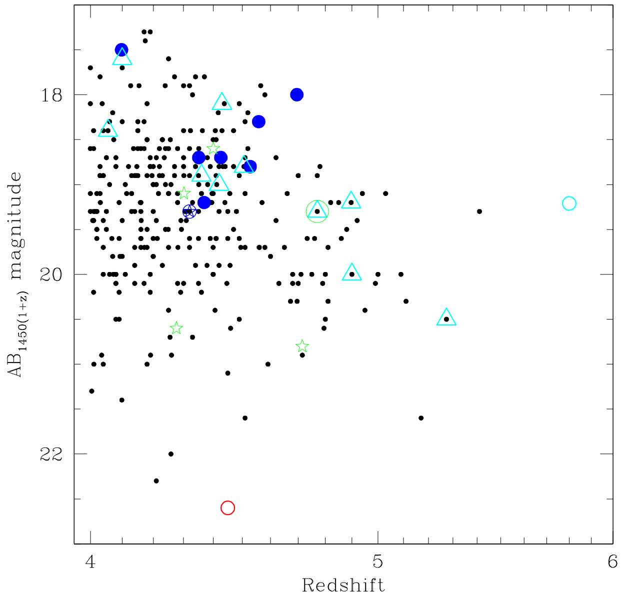

FIG. 3.— $AB_{1450(1+z)}$ magnitude versus redshift for all known $z > 4$ quasars. For objects lacking a published value of $AB_{1450(1+z)}$, the magnitude has been calculated from the published magnitudes using empirical relationships between the observed fluxes in the different filters. RQQs with *Chandra* detections are plotted as triangles, and the $z = 4.77$ RLQ SDSS 0210−0018 is shown as a circled triangle. The *ROSAT*-detected RQQs and RLQ are plotted as filled circles and a circled star, respectively. Blazars from the KBS sample are plotted as open stars. For comparison, we have plotted as open circles the $z = 4.45$ X-ray selected RQQ RX J1052+5719 (Schneider et al. 1998) and the $z = 5.80$ RQQ SDSS 1044−0125 (Fan et al. 2000b; B01). The present *Chandra* objects sample the $AB_{1450(1+z)}$ magnitude distribution well. Note the excellent capabilities of present X-ray instruments to detect high-redshift objects; in fact, the five highest-redshift objects so far detected in X-rays have been observed by *XMM-Newton* (B01) and *Chandra* (this paper).

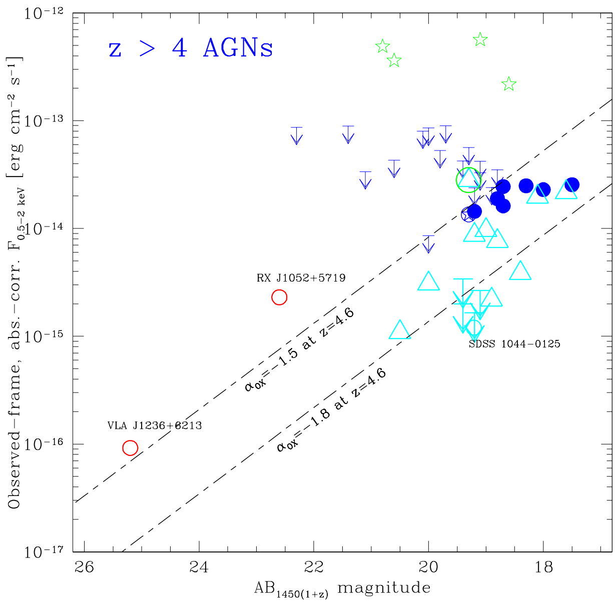

FIG. 4.— Observed-frame, Galactic absorption-corrected 0.5–2 keV flux versus $AB_{1450(1+z)}$ magnitude for $z > 4$ AGNs. Symbols are as in Fig. 3. Small arrows indicate *ROSAT* upper limits, while *Chandra* upper limits are shown as large arrows. For comparison, we have plotted as open circles the $z = 4.424$ Seyfert galaxy VLA J1236+6213 (Waddington et al. 1999; Brandt et al. 2001b), the $z = 4.45$ RQQ RX J1052+5719, and the $z = 5.80$ RQQ SDSS 1044−0125. The slanted lines show $\alpha_{ox} = -1.5$ and $\alpha_{ox} = -1.8$ loci for $z = 4.6$ (the average redshift of the present sample), assuming the same X-ray and optical spectral shapes used in the text.

errors in the low-energy ($\lesssim 0.5$ keV) calibration of the *ROSAT* PSPC. Furthermore, in a few cases, additional archival observations have been used and averaged. We also used the XIMAGE package (Giommi et al. 1992) to recalculate *ROSAT* upper limits. All the results concerning the KBS objects presented in the following are derived from this re-analysis and are shown in Table 4.

Inspection of Fig. 4 shows that the *Chandra* $z > 4$ quasars tend to lie below the *ROSAT* ones by a typical factor of ≈ 3 in X-ray flux (even within the same optical flux range). Only three *Chandra* objects, the $z = 4.77$ RLQ SDSS 0210−0018, the $z = 4.10$ RQQ PSS 1057+4555 and the $z = 4.43$ RQQ PSS 0248+1802, have X-ray fluxes comparable to those of the *ROSAT* quasars. Comparing the soft X-ray fluxes of the *Chandra* and *ROSAT* objects with $AB_{1450(1+z)}$ magnitudes in the range $\approx$ 17.5–19.5 (excluding the BALQSOs SDSS 1129−0142 and SDSS 1605−0112 and the *ROSAT* non-detections) by means of the Kolmogorov-Smirnov test, we obtain that the probability that the two samples are drawn from the same parent population is $\approx 1.8 \times 10^{-4}$. However, it is possible that some of the undetected KBS quasars in the above range of $AB_{1450(1+z)}$ magnitude are as X-ray faint as the *Chandra* objects.

Several checks have been carried out in order to try to understand this difference. We have first looked for an instrumental origin. At the present time, the *Chandra* ACIS calibration is uncertain to ≈ 15% at energies below ≈ 1 keV (R. Kilgard 2001, private communication), mainly due to potential problems in the ACIS quantum efficiency at low energies. A mis-calibration between the *ROSAT* PSPC and *Chandra* ACIS could be present as well, but it is very unlikely to be large enough to account for the observed difference of a factor of ≈ 3 in the average flux. A physical explanation for these findings thus appears more likely, although we note that significant evolution would be surprising given the small difference in the average redshifts of the two samples ($\Delta z \approx 0.2$, corresponding to a time interval of ≈ 40 Myr). Systematically different selection effects for the KBS objects and the *Chandra* objects may well play a role in causing the observed X-ray flux difference. For example, the SDSS could be more effective at finding objects that suffer from X-ray absorption or have intrinsic SEDs with weaker X-ray emission. To look for obvious selection effects, we have compared the optical emission-line properties of the *Chandra* quasars with those of KBS; the optical emission lines could be affected by reddening if absorption is present, or they could respond to a different ionizing continuum shape. No obvious correlation of the X-ray properties with the intensities of the Lyα or C IV emission lines is apparent, but the non-uniform spectral coverage of the quasars prevents us from carrying out a quantitative analysis of this issue. In addition, there are not sufficient data to search effectively for a systematic difference in the optical continuum shape.

For the *Chandra* sample, a correlation of the X-ray flux with the $AB_{1450(1+z)}$ magnitude is suggested by Fig. 4, where three out of the five X-ray faintest *Chandra* quasars (excluding the BALQSOs, which will be discussed in § 4.3) also have the faintest optical $AB_{1450(1+z)}$ magnitudes. Correlations of the X-ray flux with the optical magnitude for quasars have been extensively studied at low redshift (e.g., Zamorani et al. 1981). Applying the Spearman rank-order correlation test to the *Chan-*

TABLE 4
PROPERTIES OF $z > 4$ QUASARS ORIGINALLY PRESENTED BY KBS

Object	z	$AB_{1450(1+z)}$	M_B	f_x[a]	α_{ox}
ROSAT detections					
Q 0000−2619	4.10	17.5	−28.4	2.55	−1.71
BR 0019−1522	4.53	18.8	−27.2	1.89	−1.56
BR 0351−1034	4.35	18.7	−27.3	1.62	−1.60
BR 0951−0450	4.37	19.2	−26.8	1.44	−1.54
BRI 0952−0115	4.43	18.7	−27.3	2.45	−1.52
BR 1202−0725	4.70	18.0	−28.1	2.29	−1.63
RX J1759.4+6638	4.32	19.3	−26.7	1.35	−1.53
BR 2237−0607	4.56	18.3	−27.7	2.49	−1.58
ROSAT Upper Limits					
PC 0027+0525	4.10	21.4	−24.5	<8.93	<−0.90
PC 0027+0521	4.21	22.3	−23.6	<8.69	<−0.77
Q 0046−293	4.01	19.3	−26.5	<5.65	<−1.31
Q 0051−279	4.40	19.2	−26.8	<2.38	<−1.45
Q 0101−304	4.07	20.0	−25.9	<0.86	<−1.51
BRI 0103+0032	4.43	18.8	−27.2	<3.51	<−1.45
SDSS 033829.31+002156.3	5.00	20.0	−26.2	<8.55	<−1.10
PC 0953+4749	4.46	19.1	−26.9	<3.28	<−1.41
BRI 1050−0000	4.29	19.4	−26.5	<4.24	<−1.33
BR 1144−0723	4.15	18.8	−27.1	<2.39	<−1.52
SDSS 122600.68+005923.6	4.25	19.1	−26.8	<4.20	<−1.38
PC 1233+4752	4.45	20.1	−25.9	<8.02	<−1.11
PKS 1251−407	4.46	19.7	−26.3	<8.99	<−1.15
SDSS 131052.52−005533.4	4.14	18.9	−27.0	<2.40	<−1.51
Q 2133−4311	4.26	21.1	−24.8	<3.37	<−1.11
Q 2139−4324	4.46	20.6	−25.4	<4.30	<−1.14
PC 2331+0216	4.09	19.8	−26.3	<5.28	<−1.24
Blazars					
RX J1028.6−0844	4.28	20.6	−25.3	36.2	−0.79
GB 1428+4217	4.72	20.8	−25.3	48.9	−0.69
GB 1508+5714	4.30	19.1	−26.8	56.4	−0.94
PMN J0525−3343	4.40	18.6	−27.4	21.8	−1.18

[a] Galactic absorption-corrected flux in the observed 0.5–2 keV band in units of 10^{-14} erg cm^{-2} s^{-1}.

dra objects excluding the RLQ and the BALQSOs, we find that the correlation of the X-ray flux with the $AB_{1450(1+z)}$ magnitude is significant at the $\approx 97.3\%$ level. Including also the RQQs of the KBS sample (with the upper limits), the correlation becomes significant at the $\approx 99.9\%$ level.

4.2. *Comparison of the Spectral Energy Distributions*

To investigate whether high-redshift quasars have different SEDs with respect to lower-redshift samples, Fig. 5 plots the α_{ox} index against the luminosity density at 2500 Å for radio-quiet, optically selected samples of quasars. Following Pickering, Impey, & Foltz (1994) and B01, as comparison samples we used the Bright Quasar Survey (BQS; Schmidt & Green 1983) RQQs and the Large Bright Quasar Survey (LBQS; Hewett, Foltz, & Chaffee 1995) RQQs; the latter provides a well-defined comparison sample with a significantly higher median luminosity than that of the BQS. Further details can be found in B01 and in the caption of Fig. 5. We have recalculated both the 2500 Å luminosity densities and the α_{ox} values for the KBS sample using the same optical continuum adopted in this paper.

Obviously, the large scatter of the data points in Fig. 5, coupled with the relatively small number of high-redshift quasars thus far detected in the X-ray band, prevents us from drawing firm conclusions about an evolutionary trend of the SED. However, the KBS quasars are characterized, on average, by SEDs which resemble those of lower-redshift samples reasonably well. In contrast, the *Chandra* quasars appear to populate preferentially the region of lower α_{ox} values. The postulated steepening of α_{ox} with increasing optical luminosity (e.g., Pickering et al. 1994; Avni, Worrall, & Morgan 1995 and references therein) cannot explain these results easily, since the SDSS objects have lower optical luminosities on average than the KBS sample.

This finding can be checked in a more quantitative way by computing the average α_{ox}, taking into account the upper limits. For this purpose, we have used the ASURV software package Rev 1.2 (LaValley, Isobe, & Feigelson 1992). The optically selected RQQs observed by *ROSAT* (KBS) have $\langle\alpha_{ox}\rangle = -1.58\pm0.03$ (the quoted errors represent the standard deviation of the mean), similar to the results obtained from the $z < 0.5$ BQS excluding the Seyfert galaxies and the absorbed objects ($\langle\alpha_{ox}\rangle = -1.56\pm0.02$). The *Chandra* $z > 4$ quasars, by comparison, are characterized by a steep, more negative value of α_{ox}, with an average value of -1.78 ± 0.03 (-1.75 ± 0.03 if we exclude the two undetected BALQSOs). They lie between the *ROSAT* and BQS samples on one hand and the value obtained by B01 ($\alpha_{ox} = -1.91$) for the X-ray weak $z = 5.80$ quasar on the other. For this object intrinsic and/or associated

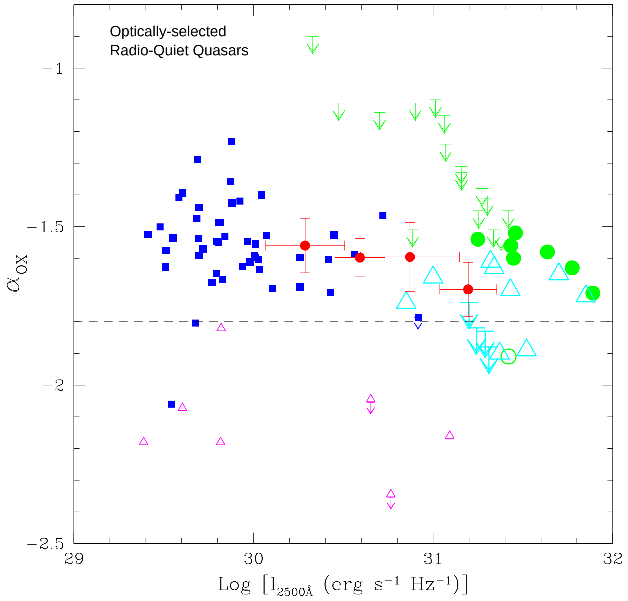

FIG. 5.— α_{ox} versus luminosity density at 2500 Å for optically selected RQQs. In particular: (1) the present *Chandra* quasars (large triangles and large upper limits); (2) the optically selected $z>4$ RQQs from KBS (large solid circles for the X-ray detected objects and small downward pointing arrows for the upper limits); (3) the $z=5.80$ SDSS X-ray weak quasar from B01 (open circle); (4) the seven luminous BQS RQQs (Schmidt & Green 1983) whose α_{ox} values and other properties indicate the presence of intrinsic absorption (small triangles, the upper limits being the quasars 0043+039 and 1700+518); (5) the other 46 luminous BQS RQQs (solid squares, one with a downward pointing arrow representing an upper limit for the quasar 1259+593); (6) the LBQS RQQs from Fig. 6b of Green et al. (1995; filled circles with error bars). The LBQS RQQ data points were derived using an X-ray counts stacking technique as described in Green et al. (1995); from left to right, these data points represent 21, 21, 35 and 70 LQBS RQQs, respectively. The three solid squares notably below the general trend (with $\alpha_{ox}\lesssim-1.8$, dashed line) are, from left to right, 2214+139, 1552+085 and 1259+593 (see B01 and Brandt, Laor, & Wills 2000 for detailed discussion).

X-ray absorption has been suggested, and recently near-infrared spectroscopy has revealed its BALQSO nature (Maiolino et al. 2001; R. W. Goodrich et al., in preparation). Similarly, X-ray absorption may be present in some of the *Chandra* quasars studied here.

The assumption of a different optical power-law continuum (e.g., α=−0.5; Richstone & Schmidt 1980) results in a slightly flatter SED for the *Chandra* sources ($\langle\alpha_{ox}\rangle=-1.75\pm0.03$). Furthermore, if we assume different X-ray spectral shapes of $\Gamma=1.7$ and $\Gamma=2.3$ (with the optical slope α=−0.79 adopted in the paper), we find $\langle\alpha_{ox}\rangle=-1.83\pm0.03$ and $\langle\alpha_{ox}\rangle=-1.73\pm0.03$, respectively.

Figure 6 shows α_{ox} versus redshift for $z>4$ *ROSAT* (KBS), *XMM-Newton* (B01) and the present *Chandra* RQQs. For comparison, α_{ox} versus redshift for lower-redshift, optically selected RQQs from the BQS and LBQS (Fig. 6d from Green et al. 1995) is also plotted. There is no clear evidence for a systematic decrease of α_{ox} with redshift in the range $z\approx4$–6. This is confirmed by the Spearman test. However, the small number of *Chandra* quasars at the highest redshifts (only three have been detected at $z\gtrsim4.8$) prevents us from drawing firm conclusions about any evolutionary trend. This issue clearly requires further investigation with larger samples of radio-quiet objects at high redshift, which will be provided by the SDSS in the next few years for X-ray follow-up with *Chandra* and *XMM-Newton*.

4.3. *Chandra undetected quasars*

The optical spectra of the 10 quasars detected by *Chandra* show no evidence of unusual properties. In contrast, three out of the four undetected objects, SDSS 1129−0142, SDSS 1532−0039 and SDSS 1605−0112, are characterized by peculiar optical (UV rest frame) properties. SDSS 1129−0142 (Zheng et al. 2000) and SDSS 1605−0112 (Fan et al. 2000a) are BALQSOs. X-ray studies at low redshift show that absorption plays a major role in hiding BALQSOs in the X-ray band (e.g., Green & Mathur 1996; Gallagher et al. 1999, 2001a,b; Brandt, Laor, & Wills 2000; Green et al. 2001). Typical H I column densities for high-ionization BALQSOs are $\approx(1\text{–}10)\times10^{22}$ cm^{-2}, while for low-ionization BALQSOs the column densities may be $\gtrsim5\times10^{23}$ cm^{-2}. Unfortunately, due to the limited optical spectral coverage at the present time, it is not possible to determine whether SDSS 1129−0142 and SDSS 1605−0112 are low-ionization BALQSOs. Even taking into account the sharp decrease of ACIS effective area above ≈5 keV, the energy band sampled by *Chandra* corresponds to the ≈2–30 keV rest-frame energy range. Therefore the non-detections of SDSS 1129−0142 and SDSS 1605−0112, coupled with their α_{ox} upper limits of −1.88 and −1.82 respectively, make them good candidates to be highly-absorbed objects, perhaps being Compton thick. Assuming the average α_{ox} of our sample excluding the BALQSOs (−1.75) and a typical X-ray slope of $\Gamma=2.0$, we infer that a non-detection is achieved for a neutral column density of $\gtrsim5\times10^{23}$ cm^{-2} for both sources. It is notable that SDSS 1044−0125 (B01), SDSS 1129−0142 and SDSS 1605−0112 all appear to have large X-ray absorbing column densities more characteristic of those seen in low-ionization BALQSOs at low redshift. Since it is unlikely a priori that all three of these objects are low-ionization BALQSOs (assuming, as at low redshift, that only $\sim1/10$ of BALQSOs are low-ionization BALQSOs), this may suggest that the X-ray absorption in high-ionization BALQSOs increases with redshift. Clearly further observations are required before firm conclusions can be drawn.

Another quasar undetected in our observations is SDSS 1532−0039 (Fan et al. 1999b, 2000a), whose optical spectrum is emission-line free. Its redshift of 4.62 has been obtained by identifying the two highly significant breaks at 6800 and 5100 Å as the onset of the Lyα forest and a Lyman limit system, respectively. The α_{ox} upper limit for this object of −1.74 marks it as moderately X-ray weak, although it need not be an extreme object. If X-ray absorption is present and is depressing the α_{ox} value, corresponding absorption in the rest-frame UV could explain the lack of observed emission lines (such a phenomenon is observed in some BALQSOs; e.g., Wills, Brandt, & Laor 1999). At present there is limited coverage of the C IV line for this object; obtaining a better signal-to-noise ratio spectrum would allow a detailed search for broad absorption lines from outflowing matter. We note that the relatively weak X-ray emission is not consistent with that expected from a BL Lac; this further supports the arguments of Fan et al. (1999b) that this object is unlikely to be a BL Lac. Anderson et al. (2001) have recently discovered two further $z>4$ quasars with anomalously weak emission lines; it will be interesting to determine if these objects are X-ray weak.

The optical spectrum of the last undetected quasar, PSS 1435+3057, shows no obvious BAL or other absorption

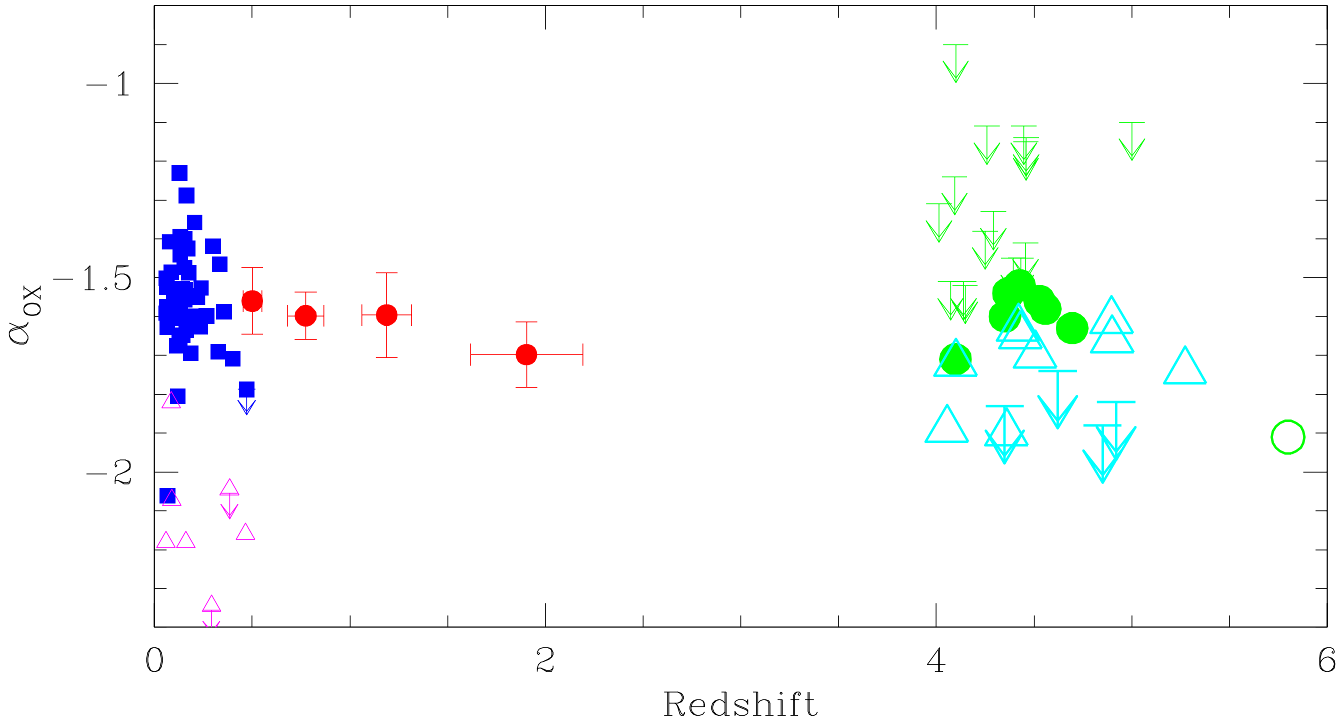

FIG. 6.— α_{ox} versus redshift for the optically selected RQQs observed by *ROSAT* (KBS, large solid circles and thin upper limits), *Chandra* (this paper, large triangles and thick upper limits), and for the $z = 5.80$ RQQ observed by *XMM-Newton* (B01, large open circle). For comparison, low-redshift RQQs are also plotted: the seven luminous and probably absorbed BQS RQQs (small open triangles), the other 46 luminous BQS RQQs (small solid squares), and the LBQS RQQs from Fig. 6d of Green et al. (1995; small filled circles with error bars, see the caption of Fig. 5 for further details). There is no evidence for a systematic decrease of α_{ox} with increasing redshift for $4 < z < 6$.

features, although the signal-to-noise ratio in the optical spectrum is low (Kennefick et al. 1995). It should be noted that this RQQ was observed for only 2.8 ks by *Chandra* .

5. REVEALING THE HIGH-REDSHIFT UNIVERSE THROUGH X-RAYS

We have found that some of the *Chandra* $z > 4$ quasars are moderately X-ray faint given their optical luminosities, by a factor of ≈ 2 with respect to the BQS sample. This effect may be due to the presence of large amounts of gas in the quasars' host galaxies fueling the active nuclei. In this regard, X-ray absorption has been detected in many $z \gtrsim 2$ RLQs and appears to increase with redshift (e.g., Elvis et al. 1994; Cappi et al. 1997; Fiore et al. 1998; Reeves & Turner 2000). That absorption could play a role in obscuring high-redshift quasars was also suggested to explain the weak X-ray emission of the $z = 5.80$ quasar SDSS 1044−0125 ($\alpha_{ox} = -1.91$; B01), which indeed was revealed to be a BALQSO (Maiolino et al. 2001; R. W. Goodrich et al., in preparation). Evidence for large amounts of gas and possibly dust in high-redshift quasars has been obtained for about one-third of the objects with multiwavelength data available. Indeed, in their study of optically selected $z > 4$ quasars from the APM sample (Irwin, McMahon, & Hazard 1991), Omont et al. (1996a) detected 240 GHz continuum emission in six out of 16 quasars. Recently Omont et al. (2001) found 1.2 mm emission from 18 out of 62 $z \gtrsim 3.8$ quasars selected from the Palomar Sky Survey (Djorgovski et al. 1998). Follow-up observations of high-redshift quasars have revealed CO emission in several cases (Ohta et al. 1996, 1998; Omont et al. 1996b; Guilloteau et al. 1997, 1999; Carilli, Menten, & Yun 1999). If the sub-mm/far-infrared emission is largely due to warm dust in the quasar host system, then molecular gas and dust masses of the order of 10^{11} and 10^{8} $M_{\odot}$, respectively, are implied in most of these systems (Benford et al. 1999; Carilli et al. 1999). Absorption by this gas may be responsible for the X-ray faintness of some of the *Chandra* quasars as well. However, the situation concerning the growth phase of massive black holes and their X-ray properties is probably complex and varied. To date there is no clear correlation between 1.2 mm detections of QSOs and their X-ray faintness; indeed, 1.2 mm observations failed to detect emission from four *Chandra* objects (SDSS 0211−0009 and SDSS 1532−0039; Carilli et al. 2001; PSS 1435+3057 and PSS 1443+2724; Omont et al. 2001), while three quasars in our sample, BRI 1033−0327, PSS 1057+4555 and PSS 1317+3531, were successfully detected (Omont et al. 1996a, 2001; Guilloteau et al. 1999).

The X-ray faintness of *Chandra* high-redshift quasars could be alternatively explained by a highly super-Eddington accretion rate for which "trapping radius" effects cause the X-rays created in the inner regions of the accretion flow to be dragged back into the black hole (e.g., Begelman 1978; Rees 1978). The accretion flow would have a luminosity of about the Eddington limit even though the mass accretion rate is super-Eddington. The low radiative efficiency associated with an accretion flow with trapping effects would allow the rapid growth of a massive black hole in the early Universe.

While the present observations directly show that *Chandra* and *XMM-Newton* can substantially increase the number of $z \approx 4$–5.3 quasars detected in the X-ray band, detailed spectroscopic studies of typical quasars at the highest redshifts

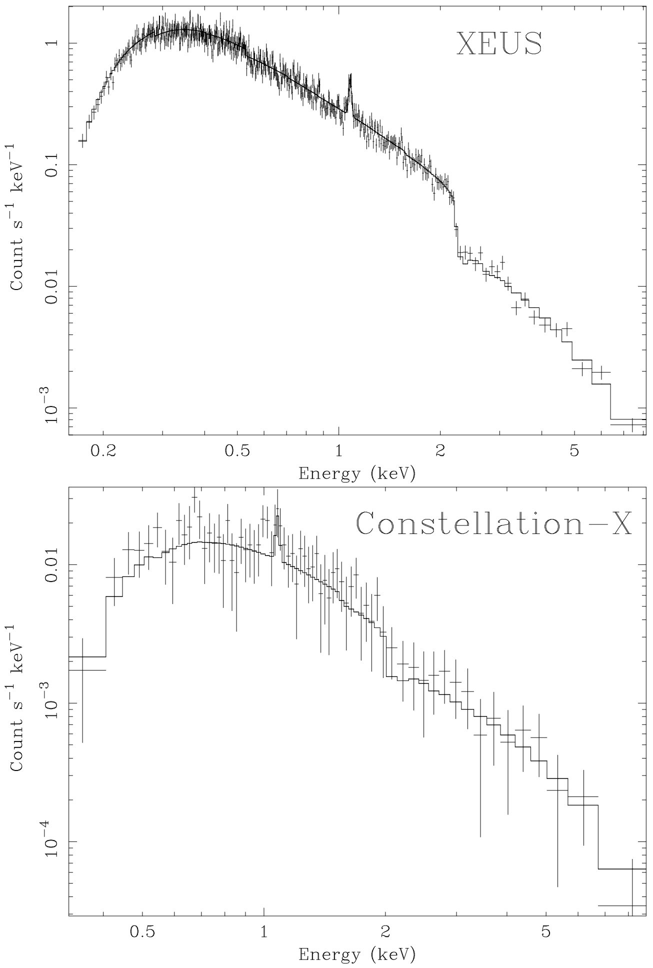

FIG. 7.— Simulated 40 ks *XEUS* (final configuration, top panel) and *Constellation-X* (bottom panel) spectra of the $z = 4.90$ quasar SDSS 0211−0009. We have used the observed 0.5–2 keV flux of 3.1×10^{-15} erg cm^{-2} s^{-1} and assumed a $\Gamma = 2$ power-law spectrum with Galactic absorption. A narrow neutral iron Kα line has been included with a rest-frame equivalent width of 140 eV.

will probably require future missions such as *Constellation-X* and especially *XEUS*. Consider, for example, the typical RQQ SDSS 0211−0009 at $z = 4.90$. Given our results on this quasar in Tables 2 and 3, *XMM-Newton* would gather $\approx$ 260 EPIC PN+MOS counts (0.2–10 keV) in a 40 ks observation; these would contrain its basic spectral properties, but spectral fitting would be limited. For comparison, 40 ks *Constellation-X* and *XEUS* observations would gather $\approx$ 860 (0.5–10 keV) and $\approx$ 31000 (0.2–10 keV) counts, respectively. In Fig. 7 we show simulated 40 ks spectra of SDSS 0211−0009 from *XEUS* (with the Cryogenic Imaging Spectrometers, final configuration) and *Constellation-X* (with the calorimeter). *XEUS* and *Constellation-X* will be able to measure the X-ray power-law photon index with an accuracy of $\approx$ 1% and $\approx$ 8%, respectively (for comparison, *XMM-Newton* can measure the photon index to $\approx$ 25%). Such measurements will allow quantitative investigation of the postulated evolution of the X-ray continua of quasars with redshift; at present, such studies are limited to objects at $z \lesssim 2.5$ where the power-law photon index may flatten by $\Delta\Gamma \approx 0.2$ between $z \approx 0$ and $z \approx 2.5$ (Vignali et al. 1999). *XEUS* can detect absorption by neutral material with a column density larger than 10^{21} cm^{-2} at the source redshift, so it should be able to probe clearly any evolution in the amount of absorption with redshift. Such absorption measurements will complement the studies being made at sub-mm and mm wavelengths, hopefully revealing the nascent material fueling black holes in their growth phase. *XEUS* will also be able to study the inner part of the accretion flow via the broad iron Kα line. Given a 6.4 keV iron Kα line with a rest-frame equivalent width of 200 eV and a width of $\sigma = 0.43$ keV (the average width obtained by Nandra et al. 1997 for a sample of Seyfert 1 galaxies), *XEUS* can measure the line energy, equivalent width, and width with an accuracy of $\approx$ 2%, $\approx$ 29% and $\approx$ 29%, respectively.

6. SUMMARY

We have presented the first results from an exploratory *Chandra* program aimed to measure the X-ray properties of the highest-redshift quasars. Ten objects were successfully detected, while four were not detected. Four of the five highest-redshift X-ray detections to date are presented in this work, and the number of $z > 4$ X-ray detected quasars has been increased by 71%. The only radio-loud quasar in the present sample, SDSS 0210−0018 ($z = 4.77$), has been serendipitously found in one of the *Chandra* fields. To date, it represents the highest-redshift RLQ detected in the X-ray band.

Combining the present results with those previously obtained for low-redshift samples, we have found that the *Chandra* quasars are on average X-ray faint (as confirmed by the optical-to-X-ray spectral index, $\alpha_{\rm ox}$). It seems likely that some of the *Chandra* $z > 4$ quasars are surrounded, during their growth phase, by large amounts of gas and dust; this matter may both feed the newly born massive black holes and weaken the X-ray emission.

We gratefully acknowledge the financial support of *Chandra* X-ray Center grant G01-2100X (CV, WNB, DPS), the Alfred P. Sloan Foundation (WNB), NSF grant PHY00-70928 and a Frank and Peggy Taplin Fellowship (XF), NASA LTSA grant NAG5-8107 (SK), NSF grant AST99-00703 (DPS), and NSF AST00-71091 (MAS). CV also acknowledges partial support from the Italian Space Agency, under the contract ASI 00/IR/103/AS, and from the Ministry for University and Research (MURST) under grant Cofin-00-02-36. We thank D. Alexander for help with IDL codes, P. Green for providing us with LBQS data, L. Townsley for the CTI correction, E. Feigelson and K. Weaver for useful discussions, and an anonymous referee for useful comments.

The Hobby-Eberly Telescope (HET) is a joint project of the University of Texas at Austin, the Pennsylvania State University, Stanford University, Ludwig-Maximillians-Universität München, and Georg-August-Universität Göttingen. The HET is named in honor of its principal benefactors, William P. Hobby and Robert E. Eberly.

REFERENCES

Anderson, S. F., et al. 2001, AJ, 122, 503
Avni, Y., Worrall, D. M., & Morgan Jr., W. A. 1995, ApJ, 454, 673
Becker, R. H., White, R. L., & Helfand, D. J. 1995, ApJ, 450, 559
Begelman, M. C. 1978, MNRAS, 184, 53
Benford, D. J., Cox, P., Omont, A., Phillips, T. G., & McMahon, R. G. 1999, ApJ, 518, L65
Blair, A. J., Stewart, G. C., Georgantopoulos, I., Boyle, B. J., Griffiths, R. E., Shanks, T., & Almaini, O. 2000, MNRAS, 314, 138
Brandt, W. N., Laor, A., & Wills, B. J. 2000, ApJ, 528, 637
Brandt, W. N., Guainazzi, M., Kaspi, S., Fan, X., Schneider, D. P., Strauss, M. A., Clavel, J., & Gunn, J. E. 2001a, AJ, 121, 591 (B01)
Brandt, W. N., et al. 2001b, AJ, 122, 1
Cappi, M., Matsuoka, M., Comastri, A., Brinkmann, W., Elvis, M., Palumbo, G. G. C., & Vignali, C. 1997, ApJ, 478, 492
Carilli, C. L., Menten, K. M., & Yun, M. S. 1999, ApJ, 521, L25
Carilli, C. L., et al. 2001, ApJ, 555, 625
Cid Fernandes, R. J., Aretxaga, I., & Terlevich, R. 1996, MNRAS, 282, 1191
Cobos Duenas, F. J., Tejada, C., Hill, G. J., & Perez, G. F. 1998, Proc. SPIE, 3355, 424
Condon, J. J., Cotton, W. D., Greisen, E. W., Yin, Q. F., Perley, R. A., Taylor, G. B., & Broderick, J. J. 1998, AJ, 115, 1693
Dickey, J. M., & Lockman, F. J. 1990, ARA&A, 28, 215
Dietrich, M., & Hamann, F. 2001, in Astrophysical Ages and Time Scales, ed. T. von Hippel, N. Manset, & C. Simpson (San Francisco: ASP), in press (astro-ph/0104180)
Djorgovski, S. G., Gal, R. R., Odewahn, S. C., de Carvalho, R. R., Brunner, R., Longo, G., & Scaramella, R. 1998, in Wide Field Surveys in Cosmology, ed. S. Colombi, & Y. Mellier (Paris: Editions Frontieres), 89
Dobrzycki, A., Ebeling, H., Glotfelty, K., Freeman, P., Damiani, F., Elvis, M., & Calderwood, T. 1999, *Chandra* Detect 1.1 User Guide
Eadie, W. T., Dryard, D., James, F. E., Roos, M., & Sadoulet, B. 1971, Statistical Methods in Experimental Physics, (Amsterdam: North-Holland)
Ebeling, H., White, D. A., & Rangarajan, F. V. N. 2001, MNRAS, submitted
Efstathiou, G., & Rees, M. J. 1988, MNRAS, 230, L5
Elvis, M., et al. 1994, ApJ, 422, 60
Fabian, A. C., Brandt, W. N., McMahon, R. G., & Hook, I. M. 1997, MNRAS, 291, L5
Fabian, A. C., Celotti, A., Iwasawa, K., McMahon, R. G., Carilli, C. L., Brandt, W. N., Ghisellini, G., & Hook, I. M. 2001a, MNRAS, 323, 373
Fabian, A. C., Celotti, A., Iwasawa, K., & Ghisellini, G. 2001b, MNRAS, 324, 628
Fan, X. 1999, AJ, 117, 2528
Fan, X., et al. 1999a, AJ, 118, 1
Fan, X., et al. 1999b, ApJ, 526, L57
Fan, X., et al. 2000a, AJ, 119, 1
Fan, X., et al. 2000b, AJ, 120, 1167
Fan, X., et al. 2001, AJ, 121, 31
Fiore, F., Elvis, M., Giommi, P., & Padovani, P. 1998, ApJ, 492, 79
Freeman, P. E., Kashyap, V., Rosner, R., & Lamb, D. Q. 2002, ApJS, 138, in press (astro-ph/0108429)
Gallagher, S. C., Brandt, W. N., Sambruna, R. M., Mathur, S., & Yamasaki, N. 1999, ApJ, 519, 549
Gallagher, S. C., Brandt, W. N., Chartas, G., & Garmire, G. P. 2001a, in Mass Outflow in Active Galactic Nuclei: New Perspectives, ed. D. M. Crenshaw, S. B. Kraemer, & I. M. George (San Francisco: ASP), in press (astro-ph/0105332)
Gallagher, S. C., Brandt, W. N., Laor, A., Elvis, M., Mathur, S., Wills, B. J., & Iyomoto, N. 2001b, ApJ, 546, 795
Gehrels, N. 1986, ApJ, 303, 336
George, I. M., Turner, T. J., Yaqoob, T., Netzer, H., Laor, A., Mushotzky, R. F., Nandra, K., & Takahashi, T. 2000, ApJ, 531, 52
Giommi, P., Angelini, L., Jacobs, P., & Tagliaferri, G. 1992, in ASP Conf. Ser. 25, Astronomical Data Analysis Software and Systems I, ed. D. M. Worrall, C. Biemesderfer, & J. Barnes (San Francisco: ASP), 100
Green, P. J., et al. 1995, ApJ, 450, 51
Green, P. J., & Mathur, S. 1996, ApJ, 462, 637
Green, P. J., Aldcroft, T. L., Mathur, S., Wilkes, B. J., & Elvis, M. 2001, ApJ, 558, 109
Guilloteau, S., Omont, A., McMahon, R. G., Cox, P., & Petitjean, P. 1997, A&A, 328, L1
Guilloteau, S., Omont, A., Cox, P., McMahon, R. G., & Petitjean, P. 1999, A&A, 349, 363
Haehnelt, M. G., & Rees, M. J. 1993, MNRAS, 263, 168
Hamann, F., & Ferland, G. J. 1999, ARA&A, 37, 487
Hasinger, G., Burg, R., Giacconi, R., Schmidt, M., Trumper, J., & Zamorani, G. 1998, A&A, 329, 482
Hewett, P. C., Foltz, C. B., & Chaffee, F. H. 1995, AJ, 109, 1498
Hill, G. J., Nicklas, H. E., MacQueen, P. J., Mitsch, W., Wellem, W., Altmann, W., Wesley, G. L., & Ray, F. B. 1998a, Proc. SPIE, 3355, 433
Hill, G. J., Nicklas, H. E., MacQueen, P. J., Tejada, C., Cobos Duenas, F. J., & Mitsch, W. 1998b, Proc. SPIE, 3355, 375
Hook, I. M., McMahon, R. G., & Shaver, P. A. 1999, in Looking Deep in the southern Sky, ed. R. Morganti, & W. J. Couch (Berlin: Springer-Verlag), 211
Kaiser, N. 1984, ApJ, 284, L9
Kaspi, S., Brandt, W. N., & Schneider, D. P. 2000, AJ, 119, 2031 (KBS)
Kaspi, S. 2001, in Probing the Physics of Active Galactic Nuclei by Multiwavelength Monitoring, ed. B. M. Peterson, R. S. Polidan, & R. W. Pogge (San Francisco: ASP), 347
Kellermann, K. I., Sramek, R., Schmidt, M., Shaffer, D. B., & Green, R. F. 1989, AJ, 98, 1195
Kennefick, J. D., de Carvalho, R. R., Djorgovski, S. G., Wilber, M. M., Dickson, E. S., Weir, N., Fayyad, U., & Roden, J. 1995, AJ, 110, 78
Kennefick, J. D., Djorgovski, S. G., & de Carvalho, R. R. 1995, AJ, 110, 2553
Kennefick, J. D., Djorgovski, S. G., & Meylan, G. 1996, AJ, 111, 1816
Kraft, R. P., Burrows, D. N., & Nousek, J. A. 1991, ApJ, 374, 344
Irwin, M., McMahon, R. G., & Hazard, C. 1991, in ASP Conf. Ser. 21, The space distribution of quasars, ed. D. Crampton (San Francisco: ASP), 117
LaValley, M., Isobe, T., & Feigelson, E. D. 1992, in ASP Conf. Ser. 25, Astronomical Data Analysis Software and Systems, ed. D. M. Worrall, C. Biemesderfer, & J. Barnes (San Francisco: ASP), 245
Lyons, L. 1991, Data Analysis for Physical Science Students, (Cambridge: Cambridge University Press)
Maiolino, R., Mannucci, F., Baffa, C., Gennari, S., & Oliva, E. 2001, A&A, 372, L5
Mathur, S. 2001, AJ, in press (astro-ph/0107163)
McMahon, R. G., Omont, A., Bergeron, J., Kreysa, E., & Haslam, C. G. T. 1994, MNRAS, 267, L9
McMahon, R. G., Priddey, S. R., Omont, A., Snellen, I., & Withington, S. 1999, MNRAS, 309, L1
Mineo, T., et al. 2000, A&A, 359, 471
Moran, E. C., & Helfand, D. J. 1997, ApJ, 484, L95
Nandra, K., George, I. M., Mushotzky, R. F., Turner, T. J., & Yaqoob, T. 1997, ApJ, 477, 602
Omont, A., McMahon, R. G., Cox, P., Kreysa, E., Bergeron, J., Pajot, F., & Storrie-Lombardi, L. J. 1996a, A&A, 315, 1
Omont, A., Petitjean, P., Guilloteau, S., McMahon, R. G., Solomon, P. M., & Pecontal, E. 1996b, Nature, 382, 428
Omont, A., Cox, P., Bertoldi, F., McMahon, R. G., Carilli, C., & Isaak, K. G. 2001, A&A, 374, 371
Ohta, K., Yamada, T., Nakanishi, K., Kohno, K., Akiyama, M., & Kawabe, R. 1996, Nature, 382, 426
Ohta, K., Nakanishi, K., Akiyama, M., Yamada, T., Kohno, K., Kawabe, R., Kuno, N., & Nakai, N. 1998, PASJ, 50, 303
Pickering, T. E., Impey, C. D., & Foltz, C. B. 1994, AJ, 108, 1542
Ramsey, L. W., et al. 1998, Proc. SPIE, 3352, 34
Rees, M. J. 1978, Phys. Scr, 17, 193
Reeves, J. N., & Turner, M. J. L. 2000, MNRAS, 316, 234
Richstone, D. O., & Schmidt, M. 1980, ApJ, 235, 361
Schmidt, M., & Green, R. F. 1983, ApJ, 269, 352
Schmidt, M., van Gorkom, J. G., Schneider, D. P., & Gunn, J. E. 1995, AJ, 109, 473
Schneider, D. P., Schmidt, M., & Gunn, J. E. 1989, AJ, 98, 1951
Schneider, D. P., Schmidt, M., & Gunn, J. E. 1991, AJ, 101, 2004
Schneider, D. P., Schmidt, M., Hasinger, G., Lehmann, I., Gunn, J. E., Giacconi, R., Trümper, J., & Zamorani, G. 1998, AJ, 115, 1230
Schneider, D. P. 1999, in After the Dark Ages: When Galaxies were Young, ed. S. Holt, & E. Smith (New York: AIP), 233
Schneider, D. P., et al. 2001, AJ, 121, 1232
Small, T. A., & Blandford, R. D. 1992, MNRAS, 259, 725
Stern, D., Djorgovski, S. G., Perley, R. A., de Carvalho, R. R., & Wall, J. V. 2000, AJ, 119, 1526
Storrie-Lombardi, L. J., McMahon, R. G., Irwin, M. J., & Hazard, C. 1996, ApJ, 468, 121
Storrie-Lombardi, L. J., Irwin, M. J., McMahon, R. G., & Hook, I. M. 2001, MNRAS, 322, 933
Townsley, L. K., Broos, P. S., Garmire, G. P., & Nousek, J. A. 2000, ApJ, 534, L139
Turner, E. L. 1991, AJ, 101, 5
Vanden Berk, D. E., et al. 2001, AJ, 122, 549
Vignali, C., Comastri, A., Cappi, M., Palumbo, G. G. C., Matsuoka, M., & Kubo, H. 1999, ApJ, 516, 582
Waddington, I., Windhorst, R. A., Cohen, S. H., Partridge, R. B., Spinrad, H., & Stern, D. 1999, ApJ, 526, L77
Warren, B. J., Hewett, P. C., Irwin, M. J., McMahon, R. G., & Bridgeland, M.T. 1987, Nature, 325, 131
Wills, B. J., Brandt, W. N., & Laor, A. 1999, ApJ, 520, L91
York, D. G., et al. 2000, AJ, 120, 1579
Yuan, W., Matsuoka, M., Wang, T., Ueno, S., Kubo, H., & Mihara, T. 2000, ApJ, 545, 625
Yun, M. S., Carilli, C. L., Kawabe, R., Tutui, Y., Kohno, K., & Ohta, K. 2000, ApJ, 528, 171
Zamorani, G., et al. 1981, ApJ, 245, 357
Zheng, W., et al. 2000, AJ, 120, 1607
Zimmermann, H. U., et al. 1998, EXSAS User's Guide, MPE Report, *ROSAT* Scientific Data Center